Sādhanā (2021) 46:30
https://doi.org/10.1007/s12046-021-01560-0

Vibration analysis of the steel shell flow tube in a vertical axial pumping station based on fluid-structure interaction (FSI) method

SHUO WANG[1,*], LIAOJUN ZHANG[1], GUOJIANG YIN[1], JIAN CHEN[2] and LI WANG[2]

[1]College of Water Conservancy and Hydropower Engineering, Hohai University, Nanjing 210098, People's Republic of China
[2]Huai'an Water Conservancy Survey and Design Research Institute Co., Ltd., Huai'an 223001, People's Republic of China
e-mail: qqwang@hhu.edu.cn; shuo.wang@ucl.ac.uk

MS received 20 November 2017; revised 29 November 2020; accepted 1 December 2020

Abstract. Design scheme of steel shell flow tube in the inflow and outflow passage of the vertical axial pumping stations takes advantages of conventional concrete scheme in simple construction and convenient installation of the pump. A three-dimensional pumping station model was established based on fluid-structure interaction method in ADINA. Typical measure points were selected to analyze the features of the unsteady turbulent flow in fluid zone and vibration responses of the steel shell tube in solid zone. Time and frequency domain investigation of fluid domain revealed the transmission path of pressure pulsation, that was the pulsation transferred from the pump to the inlet and outlet respectively with amplitudes sharply decreasing, which verified the rationality of calculation and established the basis on structure analysis. Dynamic displacement, velocity and acceleration analysis of measure points in steel shell tube showed that top shell domain near the inlet of steel shell flow tube had obvious vibration amplitude, which required great attention. The first main frequency equaled the rotational frequency of the blade, indicating one of the most important vibration sources in the pump was the pressure pulsation induced by blade rotation. The design scheme of steel shell flow tube is practical and could be promoted to other similar pumping stations because the vibration amplitude is much lower than the regularity. This research provides great importance to the design and application of the steel shell flow tube in pumping stations.

Keywords. Fluid-structure interaction; steel shell flow tube; axial pump; vibration; ADINA.

1. Introduction

Concrete structure is always adopted in the inflow and outflow passage of traditional pumping stations, which brings the problem of difficulty of construction and installation of the pump. Besides, the service life of the pumping station may be affected as the concrete is easy to crack. A creative design scheme of the steel shell flow tube was put up by the Huai'an Water Conservancy Survey and Design Research Institute Co., Ltd. to overcome the defects of the conventional concrete structure. However, thin-wall structure of the steel shell flow tube is easy to be affected by the three-dimension unsteady turbulent flow and vibrate during unit operation. As the first proof in China, the reasonability of the design of the steel shell flow tube in axial pumping station requires scientific verification and practical examination. Numerical simulation could describe the fluid flow features vividly and accurately, thus becomes one of the most promising methods for performance prediction [1–4].

Intense attention has been paid to the complex turbulent flow in the axial pump. The hub leakage and the tip clearance can lead to the tip cavitation and non-uniform flow [5, 6]. The fluid pressure pulsation is one of the main causes of vibration, noise, fissures, blade cracking and guide vanes bearing failures. Time and frequency investigation into pressure pulsation indicates that the pulsation is violent near the pump, and it decreases from blade tip to hub at the inlet of the impeller [7–11].

It is more important to perform vibration analysis due to its early detection, diagnosis and correction of the faults, which enhances both hydraulic and dynamic performance and assures safe and reliable operation of the pumping station [12]. Various methods have been adopted by scholars to explore the vibration features of the conventional concrete pumping station, such as quasi-static method, harmonic response method and the dynamic time-history method [13–16]. Usually the spatial distribution of

*For correspondence
Published online: 05 February 2021

the dynamic displacement and stress was presented, and the vibration amplitudes and safety evaluation were provided, thus corresponding vibration mitigation measures were proposed. However, there was certain difference between the gained results and the actual vibration responses because the fluid pressure pulsation adopted in their researches was artificially supposed with human factors during calculation. As one of the main vibration sources of the structure, the form of fluid pressure pulsation applied to the structure is of vital importance.

Fluid-structure Interaction (FSI) method has gained more attention in recent years, because it could not only reproduce the actual turbulent flow statue in the flow passage, but also provide the coupled effects of realistic vibration features of the structure. Relevant researches have been conducted based on FSI method [17–21]. Based on their investigation, beneficial conclusions about vibration features of the blades have been obtained: the maximum displacement occurred at impeller tip and significant stress concentration occurred in the inlet side and the contact area of the blade root and the hub. However, the pumping station was not included in their research objectives.

To overcome the above mentioned drawbacks, the main objective of the present research is to investigate the actual vibration response of the structure under the effect of unsteady turbulent flow. Based on the powerful FSI function of the large finite element software ADINA, fluid-solid coupling model was established including the steel shell flow tube, impeller and fixed guide vane. The flow and pressure condition inside the tube were analyzed to lay fundamental basis for the structural analysis. Then vibration features of the steel shell flow tube were presented and vibration safety evaluation was given.

This research is an improvement over former works with more thorough analyses and the following aspects:

(1) Two-way iterative FSI method was adopted in the calculation to obtain more actual vibration response of the structure. Shear-Stress Transport (SST) k-ω turbulence model and sliding mesh boundary condition were utilized in fluid domain to obtain actual flow condition. Newmark method was employed in solid domain to solve the oscillation equations.
(2) Creative design of steel shell flow tube in a vertical axial pumping station is the research object of the structure in current study. This steel shell flow tube is the first proof in China, which transcends conventional concrete scheme in simple construction and convenient installation of the pump. This research could not only provide theory basis for design and construction of the steel shell in axial pumping stations, but also technical support for the research and construction of subsequent similar projects.

2. Basic theory and numerical model

2.1 *Basic equations for fluid and solid domain*

Since SST k-ω turbulence model could do good performance in simulating flows around complex geometry [22] and flows with adverse pressure gradient [23], we use SST k-ω model to acquire the features of the unsteady flow in CFD calculation. SST k-ω model equations are expressed in Equations (1) and (2) [24–26].

$$\rho\frac{\partial k}{\partial t}+\rho\frac{\partial}{\partial x_j}\left(ku_j\right)=\frac{\partial}{\partial x_j}\left(\Gamma_k\frac{\partial k}{\partial x_j}\right)+\overline{G}_k-Y_k+S_k \quad (1)$$

$$\rho\frac{\partial \omega}{\partial t}+\rho\frac{\partial}{\partial x_j}\left(\omega u_j\right)=\frac{\partial}{\partial x_j}\left(\Gamma_\omega\frac{\partial \omega}{\partial x_j}\right)+G_\omega-Y_\omega+D_\omega+S_\omega \quad (2)$$

where k is the turbulent kinetic energy, ω is the turbulence dissipation rate. For other parameters including G_k, G_ω, Γ_k, Γ_ω, Y_k, Y_ω, D_ω, S_k, S_ω, the reader is referred to the reference [11].

In solid domain, linear elastic vibration equation [27] is adopted and can be written in Equation (3).

$$L^T\tau_s+\rho_s f_s=\rho_s\ddot{u} \quad (3)$$

where τ_s is the solid stress tensor, ρ_s is the solid density, f_s is the solid body force, $\ddot{u}$ is the particle acceleration vector in the solid zone, and L^T is the differential operator, which can be expressed as

$$L^T=\begin{bmatrix}\frac{\partial}{\partial x} & 0 & 0 & \frac{\partial}{\partial y} & 0 & \frac{\partial}{\partial z}\\ 0 & \frac{\partial}{\partial y} & 0 & \frac{\partial}{\partial x} & \frac{\partial}{\partial z} & 0\\ 0 & 0 & \frac{\partial}{\partial z} & 0 & \frac{\partial}{\partial y} & \frac{\partial}{\partial x}\end{bmatrix}$$

The displacement and traction on the fluid-structure interfaces should be compatible, so both the kinematic condition and the dynamic condition are applied to the fluid-structure interfaces [28]. Corresponding equations are described in Equations (4) and (5).

$$\underline{d}_f=\underline{d}_s \quad (4)$$

$$n\cdot\underline{\tau}_f=n\cdot\underline{\tau}_s \quad (5)$$

where $\underline{d}_f$ and $\underline{d}_s$ are the fluid and solid displacements, respectively, $\underline{\tau}_f$ and $\underline{\tau}_s$ denote the fluid and solid stresses, respectively. The underlining means that the definition of the value is confined to the fluid-structure interfaces only.

2.2 *Numerical model*

A FSI model of the pumping station was established in ADINA to explore its coupled vibration features. Figure 1

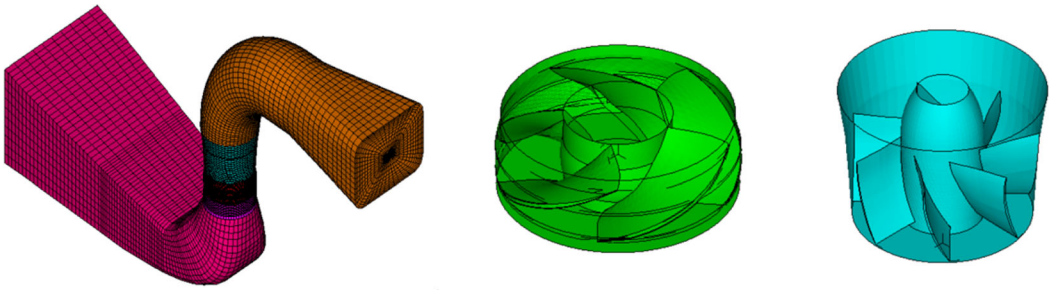

(a) Grids for integral flow passage in fluid model, guide vanes. (b) Water around impeller and (c) Water around

Figure 1. (a) Grids for integral flow passage in fluid model, (b) Water around impeller and (c) Water around guide vanes.

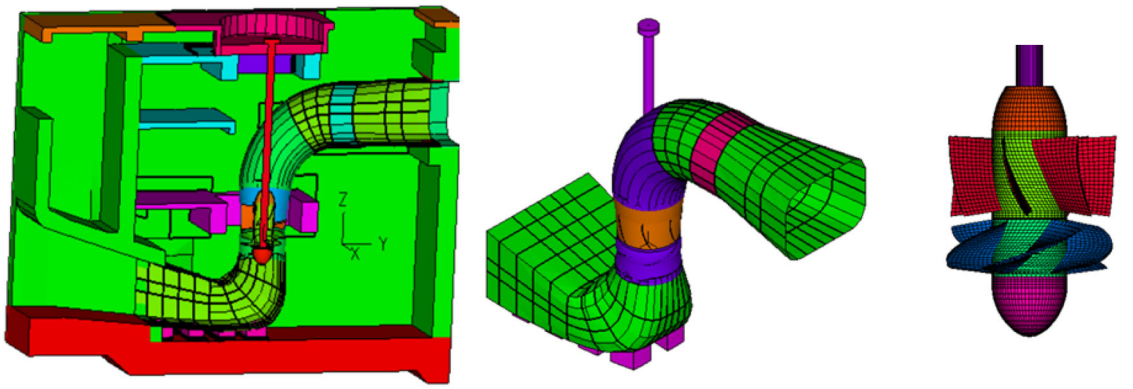

(a) Axial section of integral solid model. (b) Steel shell flow tube model, (c) Grids for impeller and fixed guide vane.

Figure 2. (a) Axial section of integral solid model. (b) Steel shell flow tube model, (c) Grids for impeller and fixed guide vane.

Table 1. Design and material parameters in FSI model.

Design parameters of the pump		Material parameters in solid model			Material parameters in fluid model	
Parameter	Value	Material	Steel	Concrete	Material	Water
Rated head H (m)	5.93	Density (kg/m^3)	7800	2400	Density (kg/m^3)	1000
Rate flow rate Q (m^3/s)	14.3	Elastic modulus (GPa)	210	28	Bulk Modulus	1e20
Rated rotation speed n (rpm)	214.3	Poisson ratio	0.3	0.2	Viscosity	0.001

shows the fluid domain, including the water in the inflow passage, the impeller chamber, the guide vane chamber, and the outflow passage. The solid model including the whole concrete structure is illustrated in figure 2(a). Since our research objective is the steel shell flow tube, large concrete structure is removed to save CPU time. Figure 2(b) shows the computational model adopted in the finite element analysis, containing steel shell flow tube, impeller, fixed guide vanes, shaft and the pier bases. Full constraints are assigned to the bottom faces of the 8 pier bases. For the circle element of the inlet and outlet section of the tube, corresponding lateral constraints are imposed. Figure 2(c) is the grid for impeller and fixed guide vane in typical section. Structured grids are adopted based on the topology of different structure. Finer grids are divided in the rotational region and field near the wall for more accurate results. Table 1 describes the design and material parameters of the pump model. Rated flow rate $Q = 14.3$ m^3/s, rated head $H = 5.93$ m, rated rotation speed $n = 214.3$ rpm, rotation frequency $f_n = 214.3/$

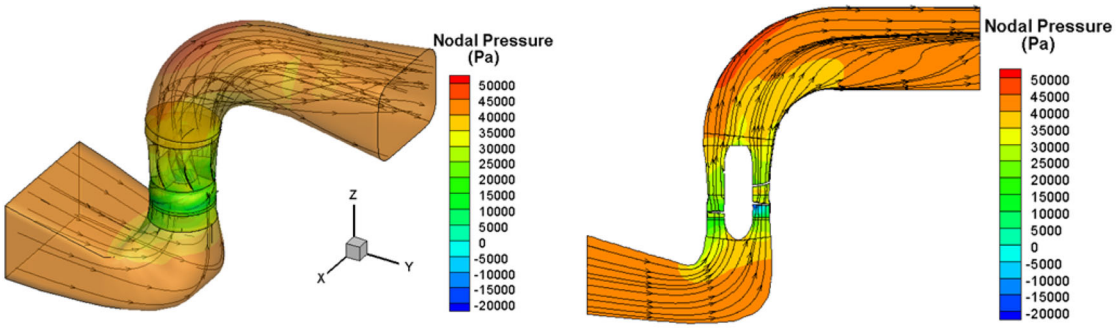

(**a**) Distribution of nodal pressure and streamlines in space. (**b**) Distribution of nodal pressure and streamlines in axial section.

Figure 3. Distribution of nodal pressure and streamlines in (a) space and (b) axial section.

60=3.57 Hz, the impeller diameter $D_2 = 1.95$ m. The number of impeller blades is 5, and the number of guide vanes is 7. In current research, the fluid-solid coupling model consists of 112931 nodes and 99662 elements in fluid region, and 37043 nodes and 28577 elements in solid region.

Here we introduce the boundary conditions for FSI calculation. Uniformly distributed velocity of 0.865 m/s is applied to the inlet in terms of the rated flow rate divided by the inlet area. Outflow is assigned to the outlet where fully developed turbulent flow is assumed. The speed of 214.3 r/min is defined on the impeller to make it rotate at every time step of calculation. The sliding mesh boundary condition is adopted in the impeller zone in order to meet the requirement of the continuity completeness and compatibility conditions along the non-conforming interfaces. FSI boundary condition is applied to the fluid-structure interfaces in fluid and solid model, respectively. The tolerance is 0.0001 in mass convergence criteria adopted in equation residual. In variable residual the tolerance is 0.001 in velocity and pressure convergence criteria. The equations are required to be converged at every time step after iteration.

As a built-in feature of the commercial software ADINA, two-way iterative FSI approach is employed to explore the vibration features of the pump. The impeller rotates at every single time step using transient analysis method in CFD module and dynamic-implicit algorithm in Structure module. The entire calculation takes 2000 steps with a time step of 0.005 s.

3. Analysis of turbulent velocity and pressure in fluid domain

The fluid pressure pulsation induced during FSI calculation has fundamental importance for vibration analysis of the steel shell flow tube structure as the fluid and solid domain are simultaneously solved in calculation process. The spiral zone and time and frequency domain analysis of fluid flow and pressure condition are conducted sequentially in this section.

3.1 *Analysis of flow condition and pressure distribution*

The flow and pressure condition of the whole flow passage at $t = 10$ s is presented in figure 3. The calculation results indicate that the static pressure varies uniformly with zero entry swirl in the inflow passage during design operation. When the flow enters the elbow section of the inflow passage, the static pressure starts to decline under the effect of the rotating impeller. The minimum static pressure and maximum dynamic pressure are both occurred in the impeller chamber because of the violent disturbance induced by the blades rotation. In the impeller chamber, the water flows along the blades and the tube wall without flow separation, and the angle between streamlines and horizontal plane remains the same. The static pressure is recovered gradually under the rectification function in the fixed guide vane region. As water enters the elbow of the outflow passage, the flow pattern remains steady and the static pressure continues to increase. While most circulation is rectified by the fixed guide vane, certain velocity circulation still occurs and the streamlines mainly deflect in the left side of the outflow tube. Overall, the flow condition in the pump is reasonable, which ensures the stable and safe operation of the pump.

3.2 *Time and frequency domain analysis of fluid pressure*

Typical measure points were selected to analyze time and frequency characteristics of pressure pulsation, as denoted in figure 4. Measure points 1 to 4 are located in the wall of steel shell tube of the inflow passage. Measure point 5 is located in the wall of water guide cone zone tube. Measure

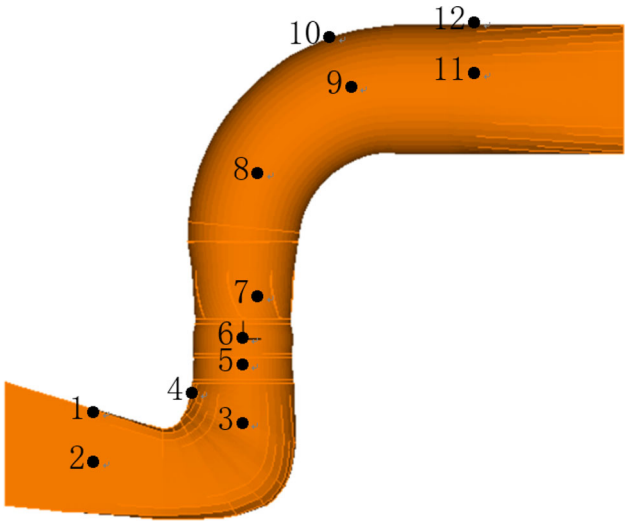

Figure 4. Measure points distribution in fluid flow passage.

point 6 is in the wall of the same height with the impeller center. Measure point 7 is in the wall of the fixed guide vane tube. Measure point 8 is in the wall of cast-iron of the outflow passage. Measure points 9 to 12 are in the wall of steel tube of the outflow passage. We focus on the time and frequency domain analysis of measure points 1 to 4, 9 to 12 as our research object is the steel shell flow tube. Pressure pulsation coefficient C_p is employed to eliminate the effect of the static pressure. The equation of C_p is as follows:

$$C_p = (p - \bar{p})/(\rho u^2/2)$$

where p is the static pressure; $\overline{p}$ is the average static pressure of one rotational cycle of blades; ρ is the water density; u is the peripheral velocity of blade tip.

Figure 5 presents time and frequency analysis of C_p of measure points 1 to 4. The wave forms of four measure points are similar, shown in figure 5(a), with a little difference in fluctuation range. Range of C_p of measure point 1 and 2 is from −0.0002 to 0.0002, which of measure point 3 and 4 is from −0.0003 to 0.0003. Frequency domain graph, illustrated in figure 5(b), indicates that the main frequency components are similar between the contraction section and elbow section of inflow passage. The first main frequency 3.57 Hz equals rotational frequency, which indicates the vibration is obviously induced by blade rotation. The amplitude is 0.00007, 0.00007, 0.00010 and 0.00012, respectively. Other main frequency component such as 7.14 Hz, twice rotational frequency, has relatively smaller amplitude. Overall, the pressure pulsation in the inflow passage is mainly affected by rotational frequency, and the amplitude becomes larger with closer distance to the pump. All amplitudes presented in figure 5(b) are less than 0.00015, so the influence of the blade's rotation is not very large.

Five measure points (8-12) are placed in outflow passage and corresponding time and frequency analysis of C_p is conducted. As demonstrated in figure 6(a), wave forms of five measure points are similar, with more second harmonic than that in inflow passage. Range of C_p of measure point 8 is from −0.0003 to 0.0003, which is larger than that of measure point 9 and 10, and larger than that of measure point 11 and 12. Investigation of frequency domain graph, shown in figure 6(b), illustrates the first main frequency is equal to rotational frequency 3.57 Hz, which is obviously affected by blade rotation. The amplitudes are 0.00013, 0.00008, 0.00008, 0.00004 and 0.00004, respectively. Other main frequency component like 7.14 Hz has relatively smaller amplitude. Therefore, the main vibration source in outflow passage is the pressure pulsation induced by rotational frequency. The pressure pulsation is sharply weakened by rectification of the fixed guide vane. Longer distance to the pump, smaller amplitude value, which is favorable to the pump.

To estimate the pressure pulsation of measure points in total and clarify the transmission path regularity of pressure

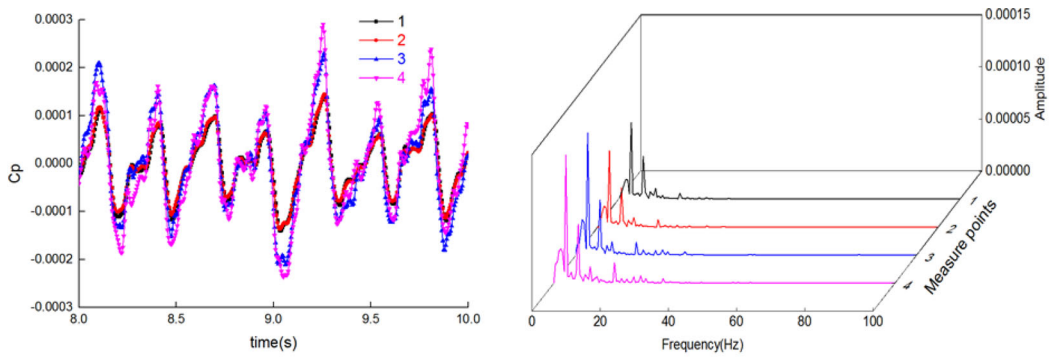

(**a**) C_p analysis of measure points 1-4 in inflow passage in time domain, (**b**) C_p analysis of measure points 1-4 in inflow passage in frequency domain.

Figure 5. C_p analysis of measure points 1-4 in inflow passage in (a) time domain and (b) frequency domain.

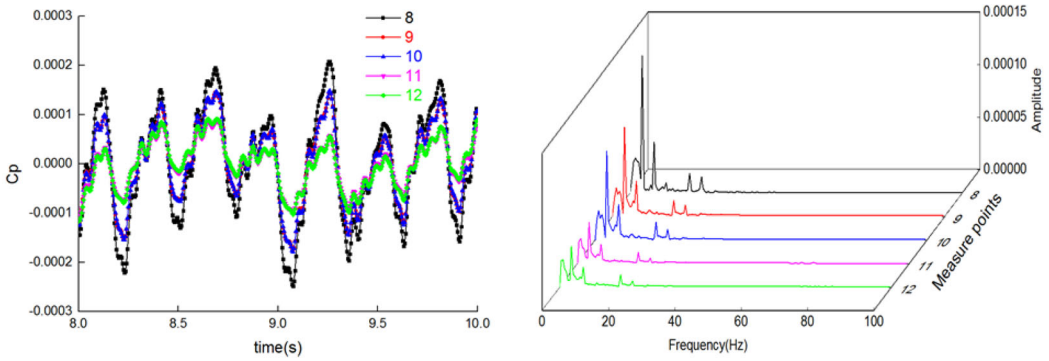

(**a**) C_p analysis of measure points 8-12 in outflow passage in time domain, (**b**) C_p analysis of measure points 8-12 in outflow passage in frequency domain.

Figure 6. C_p analysis of measure points 8-12 in outflow passage in (a) time domain and (b) frequency domain.

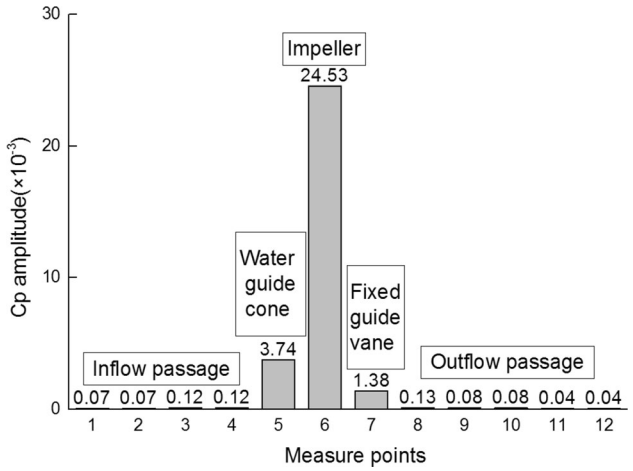

Figure 7. Comparison of C_p amplitude between all measure points.

pulsation, pulsation amplitude of each measure point is collected in figure 7. The maximum pressure pulsation amplitude reaches 0.02453 at measure point 6 in the impeller. The pulsation amplitude sharply decreases from measure point in impeller to the left and right measure points, which indicates that the pulsation transfers from pump to the inlet and outlet. The water-guide cone is obviously affected by blade rotation with an amplitude of 0.00374 at measure point 5. The pulsation induced by blade rotation plays much smaller role as the distance to the pump increases along the inflow passage and the amplitude is reduced to 0.00007 near the inlet. When analyzing the transmission of the pulsation from pump to outlet, we could find that the pulsation amplitude is greatly reduced at the measure point 7 due to the constraint function of the guide vanes. The pressure tends to be stable along flow direction in the outflow passage and the amplitude is 0.00004 near the outlet. Therefore, it is necessary to pay special attention to the inlet of the impeller chamber in future hydraulic design, as the disturbance of the blades has already existed prior to the water flowing into the impeller.

4. Vibration analysis of the steel shell flow tube

In structural vibration analysis, we use the same measure points as those in fluid flow passage to facilitate corresponding analysis. Measure points 1 to 4, 9 to 12 are selected to conduct vibration characteristics in terms of dynamic displacement, velocity and acceleration, then the safety evaluation is given.

4.1 *Dynamic displacement analysis of the steel shell flow tube*

As one of the most important indexes in vibration safety evaluation, dynamic displacement was endowed with detailed vibration limits in relevant specification. Time and frequency domain analysis of dynamic displacement of steel shell flow tube was conducted based on the fluid-solid coupling results.

Four measure points (1-4) in the inflow passage and four measure points (9-12) in straight section of the outflow tube, shown in figure 4, are selected to perform dynamic displacement analysis. Measure points of the same cross section are analyzed in the same graph for comparison. Here we only present the dynamic displacement analysis of measure points 1 and 2 in the contraction section of inflow tube for simplicity, shown in figure 8. Almost uniform fluctuation phase of the two measure points is observed in time domain graph in figure 8(a), but fluctuation ranges are largely different. The dynamic displacement range of measure point 1 is about -6 to 6 μm, whereas that of measure point 2 is -1 to 1 μm. It is mainly the location of these measure points that leads to this result: measure point 1 is in the top shell near the inlet of the inflow steel shell

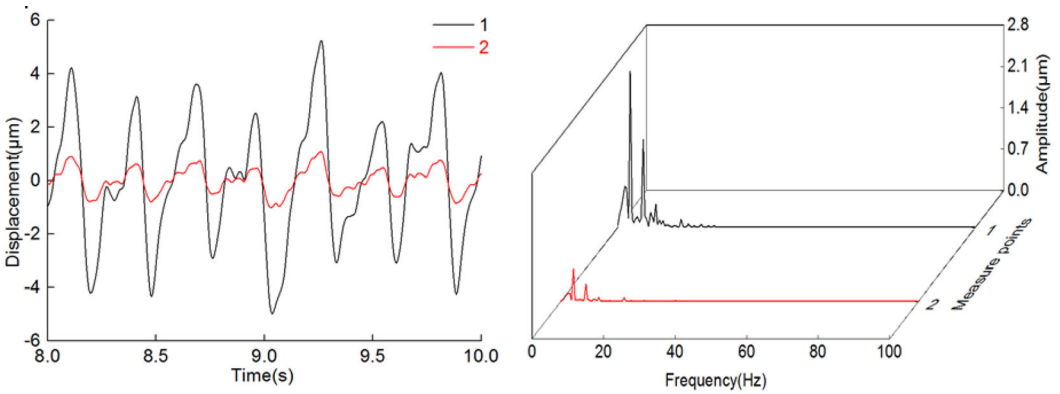

(**a**) Dynamic displacement analysis of measure points 1-2 in the contraction section of inflow tube in time domain. (**b**) Dynamic displacement analysis of measure points 1-2 in the contraction section of inflow tube in

Figure 8. Dynamic displacement analysis of measure points 1-2 in the contraction section of inflow tube in (a) time domain and (b) frequency domain.

Table 2. Dynamic displacement extreme values and first main frequency amplitudes of measure points 1-4, 9-12.

Measure point	1	2	3	4	9	10	11	12
Extreme (μm)	5.23	1.08	1.00	0.80	0.96	0.82	0.95	0.77
Amplitude (μm)	2.64	0.55	0.33	0.28	0.39	0.33	0.40	0.29

tube, where the stiffness is relatively smaller, causing wider displacement range. Frequency analysis in figure 8(b) illustrates the first main frequency of these two points is 3.57 Hz, the same as rotational frequency, which indicates that the pressure pulsation of measure point 1 and 2 is mainly induced by blade rotation. Great attention should be given to the location of measure point 1, as the amplitude of measure point 1 is 2.64 μm, which is 4.8 times that of measure point 2, 0.55 μm.

To have a whole knowledge of dynamic displacement variation of all measure points, the extreme values and first main frequency amplitudes of measure points 1-4, 9-12 are presented in table 2. Since measure point 1 is in the top shell near the inlet of the inflow steel shell tube with relatively smaller stiffness, the extreme value of dynamic displacement 5.23 μm and corresponding amplitude 2.64 μm of measure point 1 is obviously larger than that of other measure points. The calculated results of dynamic displacement are far less than the criterion value of 0.2 mm in the vibration control criterion of the hydropower house, indicating good conformance to the regularity.

4.2 *Velocity analysis of the steel shell flow tube*

Time and frequency results of the measure points 1-4 are typically plotted and analyzed in the following sections.

Figure 9 presents time history curve and frequency graph of velocity of the measure point 1 and 2 in contraction section of inflow tube. Time domain graph of velocity in figure 9(a) shows different fluctuation ranges but almost uniform fluctuation phase of measure points 1 and 2. The velocity variation of measure point 1 is from 0 to 0.2 mm/s, whereas that of measure point 2 is from 0 to 0.05 mm/s. The large difference in the pulsation range of these measure points is consistent with results of dynamic displacement. Figure 9(b) demonstrates the first main frequency of measure point 1 is 3.57 Hz with an amplitude of 0.036 mm/s. The first main frequency of measure point 2 is 10.69 Hz, three times rotational frequency, and the amplitude is 0.008 mm/s. Investigation in frequency analysis shows the velocity vibration of measure points 1 and 2 is mainly caused by blade rotation.

Time history curve and frequency graph of velocity of measure point 3 and 4 in elbow section of inflow tube is shown in figure 10. The regularity of velocity fluctuation of measure points 3 and 4 is similar, which is in accord with corresponding result of dynamic displacement. Time domain graph in figure 10 indicates the fluctuation of two measure points is from 0 to 0.07 mm/s. Frequency graph, as shown in figure 10(b), illustrates the first main frequency of these two points is 35.62 Hz, which is ten times rotational frequency and obviously induced by blades rotation. The amplitudes of first main frequency of measure point 3 and 4 are 0.013 mm/s and 0.011 mm/s, respectively.

Table 3 demonstrates velocity variation extreme and first main frequency amplitude of measure points 1-4, 9-12. Similar velocity variation regularity is observed that velocity variation extreme and amplitude of measure point 1 is obviously larger than that of other measure points with

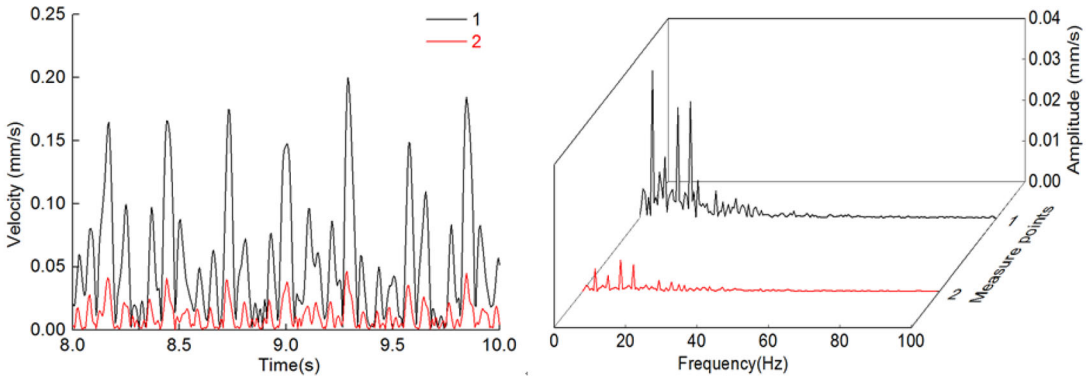

(**a**) Velocity analysis of measure points 1-2 in the contraction section of inflow tube in time domain. (**b**) Velocity analysis of measure points 1-2 in the contraction section of inflow tube in frequency domain.

Figure 9. Velocity analysis of measure points 1-2 in the contraction section of inflow tube in (a) time domain and (b) frequency domain.

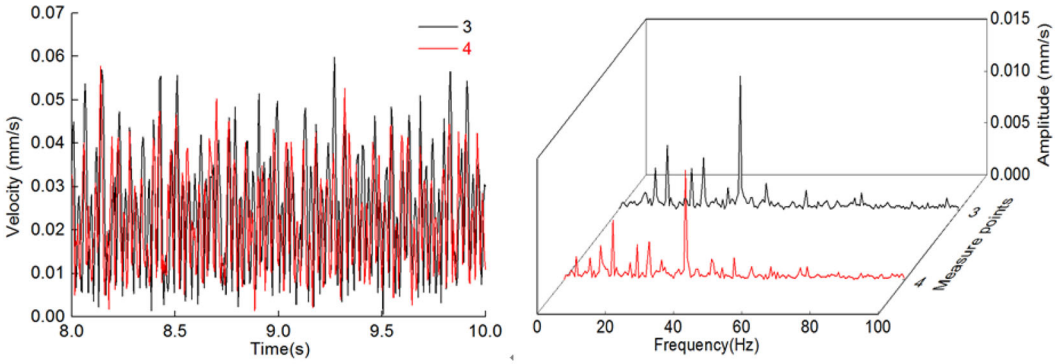

(**a**) Velocity analysis of measure points 3-4 in the elbow section of inflow tube in time domain. (**b**) Velocity analysis of measure points 3-4 in the elbow section of inflow tube in frequency domain.

Figure 10. Velocity analysis of measure points 3-4 in the elbow section of inflow tube in (a) time domain and (b) frequency domain.

Table 3. Velocity variation extreme values and first main frequency amplitudes of measure points 1-4, 9-12.

Measure point	1	2	3	4	9	10	11	12
Extreme (mm/s)	0.200	0.046	0.060	0.058	0.050	0.045	0.048	0.045
Amplitude (mm/s)	0.036	0.008	0.013	0.011	0.006	0.006	0.006	0.005

extreme value of 0.200 mm/s and amplitude of 0.036 mm/s, which are much smaller than the criterion value of 5 mm/s in the control criterion of hydropower house vibration.

4.3 *Acceleration analysis of the steel shell flow tube*

Figure 11 presents time history curve and frequency graph of acceleration of measure point 1 and 2 in contraction section of inflow tube. Large difference in fluctuation ranges presented in figure 11(a) is in conformity with corresponding results of dynamic displacement and velocity. The acceleration of measure point 1 varies from 0 to 12 mm/s^2, whereas the fluctuation of measure point 2 is 0 to 3 mm/s^2. Frequency analysis shows the first main frequency of measure point 1 is 3.57 Hz, and the amplitude is 1.450 mm/s^2. The first main frequency of measure point 2 is 49.87 Hz, fourteen times rotational frequency, and the amplitude is 0.219 mm/s^2.

Time history curve and frequency graph of acceleration of measure point 3 and 4 in elbow section of inflow tube is demonstrated in figure 12. Time domain graph in

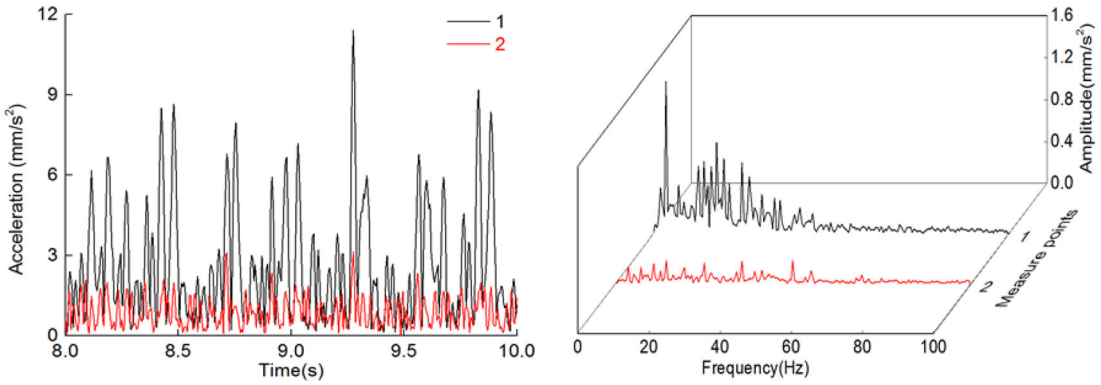

(**a**) Acceleration analysis of measure points 1-2 in the contraction section of inflow tube in time domain. (**b**) Acceleration analysis of measure points 1-2 in the contraction section of inflow tube in frequency domain.

Figure 11. Acceleration analysis of measure points 1-2 in the contraction section of inflow tube in (a) time domain and (b) frequency domain.

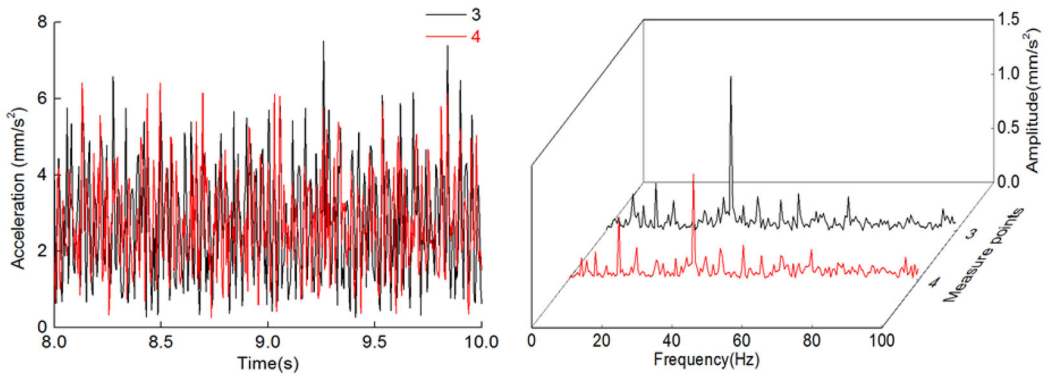

(**a**) Acceleration analysis of measure points 3-4 in the elbow section of inflow tube in time domain. (**b**) Acceleration analysis of measure points 3-4 in the elbow section of inflow tube in frequency domain.

Figure 12. Acceleration analysis of measure points 3-4 in the elbow section of inflow tube in (a) time domain and (b) frequency domain.

figure 12(a) indicates the fluctuation of each measure point is from 0 to 8 mm/s^2. Frequency graph, as shown in figure 12(b), shows first main frequency of two points is 35.62 Hz, ten times rotational frequency. The acceleration amplitudes of first main frequency of measure point 3 and 4 are 1.430 mm/s^2 and 0.974 mm/s^2, respectively.

Acceleration variation extreme and first main frequency amplitude of measure points 1-4, 9-12 are shown in table 4. Extreme value of measure point 1 is 11.41 mm/s^2, which is largest among all measure points. Amplitudes of measure point 1 and 3 are relatively higher than others with the magnitude of 1.45 mm/s^2 and 1.43 mm/s^2, respectively. The criterion value in the control criterion of hydropower house vibration is set as 1 m/s^2, which is much larger than the calculated acceleration values.

4.4 *First main stress analysis of the steel shell flow tube*

The dynamic stress is employed to eliminate the effect of the static stress. First main stress analysis of measure points 1 and 2 in the contraction section of inflow tube is presented in figure 13. Time domain graph in figure 13(a) indicates the two measure points have almost uniform fluctuation phase and fluctuation ranges are from −15 kPa to 15 kPa. The wave crest of measure point 2 is a little higher and wave trough is a little lower than that of measure point 1. Frequency domain graph illustrated in figure 13(b) shows the main frequencies are 3.57 Hz, 7.14 Hz, 10.71 Hz, several times rotational frequency 3.57 Hz, which indicates the pressure pulsation of measure point 1 and 2 is mainly induced by blade rotation. All

Table 4. Acceleration variation extreme values and first main frequency amplitudes of measure points 1-4, 9-12.

Measure point	1	2	3	4	9	10	11	12
Extreme (mm/s^2)	11.41	3.15	7.50	6.41	4.88	4.64	4.86	4.63
Amplitude (mm/s^2)	1.45	0.22	1.43	0.97	0.65	0.65	0.72	0.61

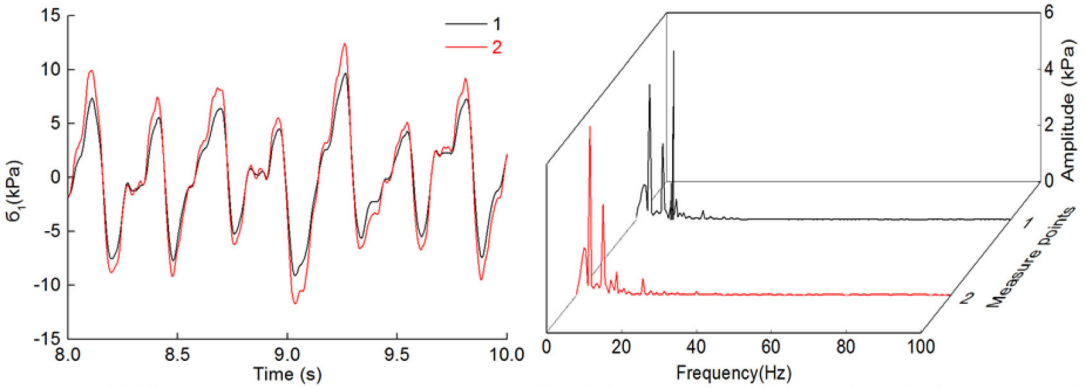

(**a**) First main stress analysis of measure points 1-2 in the contraction section of inflow tube in time domain. (**b**) First main stress analysis of measure points 1-2 in the contraction section of inflow tube in frequency domain.

Figure 13. First main stress analysis of measure points 1-2 in the contraction section of inflow tube in (a) time domain and (b) frequency domain.

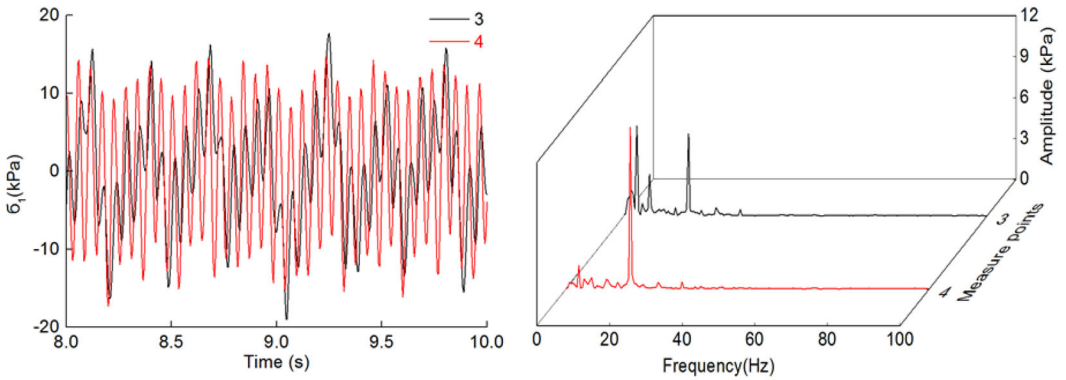

(**a**) First main stress analysis of measure points 3-4 in the elbow section of inflow tube in time domain. (**b**) First main stress analysis of measure points 3-4 in the elbow section of inflow tube in frequency domain.

Figure 14. First main stress analysis of measure points 3-4 in the elbow section of inflow tube in (a) time domain and (b) frequency domain.

amplitudes are less than 6 kPa, showing not large impact of blade rotation.

Figure 14 presents first main stress analysis of measure points 3 and 4 in the elbow section of inflow tube. The wave forms of these two measure points are not alike due to their different side location. Time domain graph shown in figure 14(a) indicates both fluctuation ranges are from −20 kPa to 20 kPa. Frequency analysis in figure 14(b) demonstrates the main frequency of measure point 3 is 3.57 Hz and 17.86 Hz, one and five times blade rotational frequency, and corresponding amplitude is 6.57 kPa and 6.03 kPa, respectively. First main frequency of measure point 4 is 17.81 Hz with an amplitude of 11.86 kPa.

Table 5 shows the extreme values and first main frequency amplitudes of the first main stress of all measure points. Relatively larger variation extreme is attained at measure point 3 and 4 with magnitude of 18.98 kPa and

Table 5. First main stress extreme values and first main frequency amplitudes of measure points 1-4, 9-12.

Measure point	1	2	3	4	9	10	11	12
Extreme (kPa)	9.69	12.42	18.98	17.29	4.84	1.44	4.77	8.41
Amplitude (kPa)	6.76	6.26	6.57	11.86	2.50	0.74	2.20	2.35

17.29 kPa, respectively. The first main frequency amplitude reaches maximum at measure point 4 with a value of 11.86 kPa, which is much larger than others.

5. Conclusions

In this research, FSI simulation has been performed by integrating fluid flow model to the mechanics and the steel shell tube model to investigate the vibration response of the steel shell flow tube in design condition. Firstly, flow condition in a vertical axial pump was analyzed using the SST k-ω turbulence model under transient state, then the dynamic displacement, velocity, acceleration and the first main stress of the steel shell flow tube were explored based on the dynamic-implicit algorithm and the two-way iterative FSI approach. The following conclusions can be drawn by analysis of the results:

1) Fluid results indicate the transmission path of pressure pulsation in the whole flow passage. The maximum pressure coefficient amplitude is 0.02453, appearing in the impeller region. The pulsation transfers from the pump to the inlet and outlet respectively, with pulsation amplitudes sharply decreasing. The amplitude is only 0.00007 near the inlet and 0.00004 near the outlet. Frequency domain analysis shows the blade rotation is the main vibration source in the whole flow passage. Overall, transmission path of the pressure pulsation is rational, which lays the basis for the vibration analysis of the steel shell flow tube.
2) Steel shell flow tube results show that measure point 1 is most sensitive to the turbulent flow, which gets the maximum pulsation amplitude of dynamic displacement, velocity and acceleration. The dynamic displacement of measure point 1 ranges from -6 to 6 μm, with the first main frequency amplitude of 2.64 μm. Dynamic displacement amplitudes in other regions of the inflow and outflow steel tube are much smaller. Velocity fluctuates from 0 to 0.2 mm/s, with the amplitude of 0.036 mm/s. The variation of acceleration is from 0 to 12 mm/s^2 and the amplitude is 1.450 mm/s^2. Frequency domain analysis shows the first main frequency of all calculated vibration variables of measure point 1 equals rotational frequency 3.57 Hz, which illustrates one of the most important vibration sources in the pump was the pressure pulsation induced by blade rotation. Measure points 3 and 4 present larger dynamic stress, and the amplitudes are less than 20 kPa. Great importance should be attached to the top shell domain near the inlet of steel shell flow tube, as it has obvious dynamic displacement, velocity and acceleration amplitude.
3) The vibration amplitudes are much lower than the criterion value in regularity, so the design scheme of steel shell flow tube is reasonable and practical. The conclusion that this steel shell flow tube scheme could be promoted to the design and construction of pumping stations of similar type could be drawn.

Acknowledgements

This work was financially supported by the National Key Research and Development Program of China (Grant No. 2017YFC0404903), the Fundamental Research Funds for the Central Universities (Grant No. 2016B41014) and the Priority Academic Program Development of Jiangsu Higher Education Institutions (PAPD). The authors are very grateful to the Institute of Hydraulic Structure for providing us with the high-performance server for calculation.

References

[1] Shah S R, Jain S V, Patel R N and Lakhera V J 2013 CFD for centrifugal pumps: a review of the State-of-the-Art. *Proc. Eng.* **51** 715–720
[2] Li D Y, Wang H J, Xiang G M and Gong R Z 2015 Unsteady simulation and analysis for hump characteristics of a pump turbine model. *Renew. Energy.* **77** 32–42
[3] Jafarzadeh B, Hajari A, Alishahi M M and Akbaria M H 2011 The flow simulation of a low-specific-speed high-speed centrifugal pump. *Appl. Math. Modell.* **35** 242–249
[4] Choi H J, Zullah M A, Roh H W, Ha P S, Oh S Y and Lee Y H 2013 CFD validation of performance improvement of a 500kW Francis turbine; *Renew. Energy.* **54** 111–123
[5] Zhang D S, Shi W D, Chen B and Guan X F 2010 Unsteady flow analysis and experimental investigation of axial-flow pump; *J.Hydrodyn.* **22** 35–43
[6] Zhang D S, Shi W D, Esch B P M, Shi L and Dubuisson M 2015 Numerical and experimental investigation of tip leakage vortex trajectory and dynamics in an axial flow pump. *Comput. Fluids.* **112** 61–71

[7] Dong X, Guo Y, Bi Z, Li Y B and Cheng X R 2015 Internal and external characteristics of axial-flow pump based on coupling CFX with Workbench. *J. Drain. Irrig. Mach. Eng.* **33** 488–493

[8] Zhang Y X, Wang X Y, Ding P and Tang X L 2014 Numerical analysis of pressure fluctuation of internal flow in submersible axial-flow pump. *J. Drain. Irrig. Mach. Eng.* **32** 302–307

[9] Zhang D S, Pan D Z, Shi W D and Zhang G J 2014 Numerical simulation of cavitation flow in axial flow pump and induced pressure fluctuation. *J. Huazhong Univ. Sci. Technol.* **17** 423–428

[10] Shi W D, Zhang G J, Zhang D S, Wu S Q and Xu Y D 2014 Effects of non-uniform suction flow on performance and pressure fluctuation in axial-flow pumps. *J. Drain. Irrig. Mach. Engi* **32** 277–282

[11] Wang S, Zhang L J and Yin G J 2017 Numerical investigation of the FSI characteristics in a tubular pump. *Math. Probl. Eng.* **2017** 1–9

[12] Abu-Zeid M A and Abdel-Rahman S M 2013 Bearing problems' effects on the dynamic performance of pumping stations. *Alexandr. Eng. J.* **52** 241–248

[13] Ye X and Ding X T 2016 Vibration characteristics and resistance of structures of third Huaian pumping station. *Adv. Sci.Technol. Water Resour.* **36** 86–89

[14] Wang X, Li T C and Pan S J 2008 Vibration analysis of the pump-house of the third Huaiyin Pumping Station. *Adv. Sci. Technol. Water Resour.* **28**(5) 49–53

[15] Wang X 2008 Research on submarine cable shield insulation in Hainan interconnection project. *Water Resour. Power.* **26**(5) 178–181

[16] Li Y Y, Gao F, Li Q H and Yang K K 2014 Computing method of vibration in large bulb tubular pump system. *Adv. Sci. Technol. Water Resour.* **34**(5) 69–74

[17] Shi W D, Wang G T, Zhang D S, Jiang X P and Xu Y 2013 Stress characteristics in blades of axial-flow pump based on fluid-structure interaction. *J. Draina. Irrig. Mach. Eng.* **31** 737–740

[18] Zhang X, Zheng Y, Mao X L, Wu Z Q, Kan K and Mou T 2014 Strength analysis of axial flow pump impeller based on fluid solid coupling. *Water Resourc.Power.* **32**(7) 137–139

[19] Tang X L, Jia Y X, Wang F J, Zhou D Q, Xiao R F, Wu Y L and Liu Z Q 2013 Turbulent flows in tubular pump and fluid-structure interaction characteristics of impeller. *J. Drain. Irrig. Mach. Eng.* **31** 379–383

[20] Shi W D, Wang G T, Jiang X P, Zhang D S, Yun Q L and Xu Y 2012 Numerical calculation for effect of fluid-structure interaction on flow field in axial-flow pump. *Fluid Machi.* **40**(1) 31–34

[21] Shang W, Liao W L and Zheng X B 2009 Strength of axial flow blades considering fluid-structure interaction. *Journal of Hohai University.* **37**(4) 441–445

[22] Li J, Zhong C W, Pan D X and Zhuo C S 2016 A gas-kinetic scheme coupled with SST model for turbulent flows. *Comput. Math. Appl.* **78**(4) 1227–1242

[23] Kim S J, Jung J S and Kang S 2015 Fully three-dimensional Reynolds-averaged Navier-Stokes modeling for solving free surface flows around coastal drainage gates. *J. Hydro-environ. Res.* **13** 121–133

[24] Menter F R 1993 Zonal two equation k-w turbulence models for aerodynamic flows. *Recon Technical Report N.* **93** 1–21

[25] Menter F R, Kuntz M and Langtry R 2003 Ten years of industrial experience with the SST turbulence model. *Turbulence.* **2003** 1–8

[26] Menter F R 2009 Review of the shear-stress transport turbulence model experience from an industrial perspective. *Int. J. Comput. Fluid Dyn.* **23** 305–316

[27] Pálfalvi A 2010 Efficient solution of a vibration equation involving fractional derivatives. *Int. J. Non-Linear Mech.* **45** 169–175

[28] Wei S H and Zhang L J 2010 Vibration analysis of hydropower house based on fluid-structure coupling numerical method. *Water Sci. Eng.* **3** 75–84